Bilayer Edges Catalyze Supported Lipid Bilayer Formation

Kimberly L. Weirich,[†] Jacob N. Israelachvili,[†‡] and D. Kuchnir Fygenson[†§*]
[†]Biomolecular Science and Engineering Program, [‡]Chemical Engineering Department, and [§]Physics Department, University of California, Santa Barbara, California

ABSTRACT Supported lipid bilayers (SLB) are important for the study of membrane-based phenomena and as coatings for biosensors. Nevertheless, there is a fundamental lack of understanding of the process by which they form from vesicles in solution. We report insights into the mechanism of SLB formation by vesicle adsorption using temperature-controlled time-resolved fluorescence microscopy at low vesicle concentrations. First, lipid accumulates on the surface at a constant rate up to ~0.8 of SLB coverage. Then, as patches of SLB nucleate and spread, the rate of accumulation increases. At a coverage of ~1.5 × SLB, excess vesicles desorb as SLB patches rapidly coalesce into a continuous SLB. Variable surface fluorescence immediately before SLB patch formation argues against the existence of a critical vesicle density necessary for rupture. The accelerating rate of accumulation and the widespread, abrupt loss of vesicles coincide with the emergence and disappearance of patch edges. We conclude that SLB edges enhance vesicle adhesion to the surface and induce vesicle rupture, thus playing a key role in the formation of continuous SLB.

INTRODUCTION

One of the few biological universals, the lipid bilayer defines the aqueous volumes of and within all cells. Its key properties, such as susceptibility to fusion and poration, derive from the bilayer being a two-dimensional fluid with a hydrophobic core. Understanding the mechanics and dynamics of this unusual material is an essential step toward deciphering and engineering membrane-linked processes in cells, such as adhesion (1), morphogenesis (2), and ion transport and mechanosensing (3). In addition, the ability to control lipid bilayer formation and quality is fundamental to studying the structure and function of proteins that permeate or bind to cell membranes (4).

Lipid bilayers supported on solid substrates (SLB) were introduced in the mid 1980s by Brian and McConnell (5) and Tamm and McConnell (6) as an easily imaged and chemically accessible platform for studying membrane-proteins and interactions with other membranes. Today, SLBs are also finding application as surface coatings for microfluidic devices (7) and medical implants (8) due to their intrinsic biocompatibility. However, use has been limited because of difficulty achieving high quality SLBs in arbitrary solution and substrate conditions.

The most controlled way to produce SLBs is the Langmuir-Blodgett method, in which lipid monolayers are transferred to a substrate from an air-water interface by repeated passages (6). This delicate technique is not suitable for investigating proteins embedded in bilayer (9) or for mass production. A simpler way to produce single SLBs is by the adsorption and rupture of vesicles on silica (10–13) and mica (14–16). This method is scalable and amenable to embedded proteins, but markedly sensitive to solution conditions and substrates. SLB formation via vesicles is an interesting case of adsorption, where the adsorbate (vesicle) must undergo a conformation change and fuse with neighbors to create the final product. Understanding the mechanism is crucial to increasing SLB use and has motivated a variety of studies. SLB formation has been observed at the single vesicle level, using fluorescence microscopy (17,18) and atomic force microscopy (AFM) (12,15,16,19,20), as well as in bulk, using quartz crystal microbalance with dissipation (QCM-D) (10,15,21–24), surface plasmon resonance (22,23), ellipsometry (13,15,25), and x-ray (26) and neutron (27) reflectivity.

Microscopy-based experiments suggest that vesicles adsorb and fuse, reaching a critical size before rupturing (17); they also suggest that the hydrophobic edges of bilayer patches promote further rupture (16–19). Such mechanistic insights, gained on the single vesicle level, have yet to be reconciled with bulk measurements, especially those using QCM-D (19,21–24), which suggest that vesicles must reach a critical surface density before rupturing.

In this study, we report the use of fluorescence microscopy and a simple flow cell setup to observe SLB formation via vesicle adsorption over ~40,000 μm^2 in real-time with ~0.5 μm spatial resolution. Our observations bridge the gap between single vesicle and bulk techniques and help reconcile the two. In particular, our observations suggest that SLB edges are high-affinity surfaces for vesicle adsorption whose rapid disappearance, upon SLB patch coalescence, explains the characteristic decay of QCM-D signals without invoking a critical vesicle density.

MATERIALS AND METHODS

Vesicle preparation

Small unilamellar vesicles were made from synthetic 1,2-dimyristoyl-*sn*-glycero-3-phosphocholine (DMPC) and fluorescent headgroup labeled

Submitted June 26, 2009, and accepted for publication September 24, 2009.

*Correspondence: deborah@physics.ucsb.edu

Editor: Peter Hinterdorfer.

0006-3495/10/01/0085/8 $2.00

doi: 10.1016/j.bpj.2009.09.050

1,2-dimyristoyl-*sn*-glycero-3-phosphoethanolamine-*N*-(7-*nitro*-2-1,3-benzoxadiazol-4-yl) (DMPE-NBD; Avanti Polar Lipids, Alabaster, AL) without further purification via a standard protocol (28). DMPE-NBD was added to DMPC in chloroform at a lipid mass ratio of 3:100. The chloroform was evaporated under a stream of dry, filtered nitrogen gas, to leave a lipid film on the wall of a clean glass vial. To remove residual chloroform, the vial was placed in a clean desiccator (Dry Seal; Wheaton, Millville, NJ) and pumped on for 24 h with an oil-free diaphragm vacuum pump (Gast, Benton Harbor, MI).

Lipid was brought to a concentration of 4 mg/mL in pH 7.5 buffer (8.5 mM NaH_2PO_4, 1.5 mM Na_2HPO_4, 140 mM NaCl) by vortexing for ~1 min. The resulting suspension was then repeatedly frozen by submersion in liquid nitrogen and thawed in a ~60°C water bath a total of 10 times. The suspension was then forced through a series of single membranes (25 mm diameter; Anodisc, Whatman, United Kingdom) with decreasing pore sizes (200 nm, 100 nm, and 20 nm), 10 times each, using a Lipex Thermobarrel Extruder (Northern Lipids, Vancouver, Canada) connected to a tank of nitrogen gas at ~100 psi and held well above the gel transition temperature of DMPC by water circulating from a 50°C bath. The extruder hardware was rinsed with ethanol and water immediately before assembly and flushed with >15 mL buffer after installation of each new membrane. Teflon tape wrapped around the stainless steel extruder outlet prevented wetting and the associated loss of extruded suspension. Vesicles in the extruded suspension had an average diameter of ~50 nm as determined by dynamic light scattering (BI-200SM; Brookhaven Instruments, Holtsville, NY) using a 1 μm dust cutoff and an exponential correlation function.

After extrusion, the suspension was diluted to 25.8 μM (0.017 mg/mL) in buffer and stored at 4°C until use. At this low stock concentration measurable aspects of SLB formation were independent of the age of the stock. By contrast, when extruded suspensions were stored at 2 mg/mL and 4°C, the maximum intensity reached, I_{max}, decreased systematically over the course of 12 h (see the Supporting Material).

The stock vesicle suspension was further diluted immediately before use and kept on ice while data were taken. The relative lipid concentration of each diluted suspension was determined based on its fluorescence intensity at 540 nm (ND3100; Nanodrop, Wilmington, DE) averaged over nine independent measurements. The conversion between fluorescence intensity and absolute lipid concentration was determined using a colorimetric assay adapted from the literature (29–32). Absorbance was calibrated by a linear fit to a serial dilution of known DMPC concentration (see the Supporting Material).

Glass cleaning

Borosilicate glass vials and beakers (Pyrex, Corning, NY) were soaked in 0.1 M HCl for at least 4 h, rinsed copiously with pure water (milliQ; Millipore, Billerica, MA), flushed with chloroform, and dried under a stream of dry nitrogen gas before use. Between sequential experiments, beakers were rinsed with pure water and pure ethanol (200 proof; Rossville Gold Shield, Hayward, CA), and dried with dry nitrogen gas.

Borosilicate glass coverslips (No. 1, 24 × 50 mm Fisherbrand; Fisher Scientific, Pittsburg, PA) were rinsed with pure ethanol, pure water, pure ethanol again, and dried under a stream of dry nitrogen gas. Coverslips were then exposed to UV/ozone (UVOCS, Montgomeryville, PA) for 30 min to break down residual organics and immediately placed under vacuum in a dry-seal glass desiccator. All glass was used within 1 day of cleaning.

Concentration and temperature control

For every experiment, both bulk lipid concentration and solution temperature were held constant by continuously flowing the vesicle suspension through a homemade flow cell (Fig. 1). The flow channel was defined by a groove in a Teflon block pressed against a borosilicate coverslip. Borosilicate glass was studied (instead of the more common silica) because it is less brittle and so widely used in microscopy as a coverslip material. Two holes through the block at either end of the groove served as inlet and exit reservoirs. The coverslip was supported by a brass platform. Because of the extreme hydrophobicity of Teflon, light pressure, from four screws holding the block against the platform, sufficed to prevent leaks.

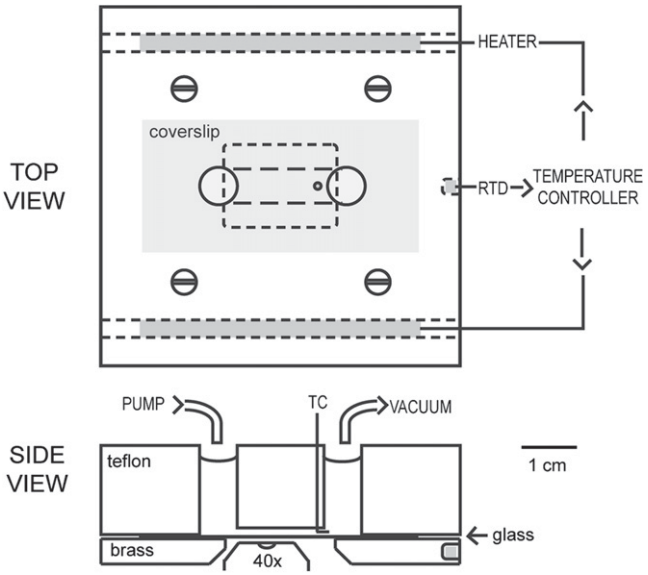

FIGURE 1 Schematics of sample flow cell drawn to scale. The flow chamber is defined by a Teflon channel pressed against a borosilicate coverslip and secured with four screws to a brass platform that rests on the stage of an inverted microscope. Sample solution drips into one reservoir and is removed at the rim of the other reservoir, allowing gravity to drive flow through the 1 mm-deep channel. Sample temperature is monitored via a thermocouple inserted downstream from the observed region. Temperature is maintained by cartridge heaters in the brass platform on either side of the channel using a PID temperature controller and RTD.

Constant temperature was important both during and after SLB formation to avoid structural changes in the SLB (6) and focal drift. Temperature control was achieved via the platform, which contained a pair of cartridge heaters (CSS01235/120; Omega Engineering, Stamford, CT) aligned parallel to the channel and an RTD (RTD-1-1PT100GX0578-36-T; Omega) equidistant between the heaters. These were connected to a temperature controller (CN7732-3PV; Omega) that maintained 29.5 ± 0.3°C during the experiments, as measured by a thermocouple (5TC-TT-E-36-36; Omega) in the flow channel. The thermocouple sat ~1 cm downstream from the imaged regions (so as to minimize its effect on flow in the field of view). The set temperature was chosen to be well above the main transition temperature for DMPC and easy to maintain with passive cooling.

Microscopy

The flow cell was assembled with a clean coverslip in a laminar flow hood, filled immediately with buffer and transferred to the microscope such that buffer circulated through the system within 5 min of assembly. A peristaltic pump (Minipuls2; Gilson, Middleton, WI) drove solution at ~50 μL/min, through silicone tubing (inner diameter = 0.76 mm, 39–664; Rainin, Oakland, CA) with a Teflon tubing tip, to the inlet reservoir. An oil-free vacuum pump (Gast) drew solution, through similar tubing, from the exit reservoir to a waste container.

Epifluorescence images were taken using an inverted microscope (IX70; Olympus, Tokyo, Japan) with a 40×/0.7 NA objective (Olympus) and a CCD camera (Sensicam-QE; Cooke Corp., Romulus, MI). The sample was illuminated by an LED (λ = 460–490 nm, LXHL-LB5C; Philips Lumileds, San Jose, CA) running on 100 mA (~0.35 mW, measured at the objective). Light passed through a filter cube composed of a 470 ± 20 nm bandpass excitation, diagonal 500 nm longpass dichroic, and 510 nm

longpass emission filters (QMAX EX450-490, XF2077, XF3086; Omega Optical, Brattleboro, VT). A shutter (Uniblitz; Vincent Associates, Rochester, NY) between the LED and the cube triggered the camera and limited the exposure of the sample to 250 ms per image.

Heating began after buffer was flowing. Imaging began after temperature stabilized (15–30 min). At least six frames were imaged under flowing buffer to measure the camera dark level. Then, the buffer was replaced with the dilute vesicle suspension. Images were collected at 20-s intervals until focus was established, and 1–10-min intervals thereafter (depending on lipid concentration) to minimize photobleaching. After SLB formation, images were taken at 3-min intervals.

Once SLB formation was complete, the flowing vesicle suspension was replaced with buffer to rinse away the fluorescence signal from the bulk; ~45 min after initiating the rinse, a spot was bleached by reducing an aperture in the illumination path and increasing the LED current to 650 mA (~1.9 mW). The spot was bleached for 60 s, the LED current was returned to 100 mA, and normal imaging resumed. Immediately after the current jumps, the LED temperature (monitored on a chart recorder (Datachart 2000; Monarch Instrument, Amherst, NH) via thermocouple) was allowed to stabilize to ensure constant intensity during bleaching and imaging.

RESULTS

Fluorescence video microscopy reveals distinct stages in the process of SLB formation via vesicle adsorption (Fig. 2; see Movie S1). At first, vesicles adsorbing to the borosilicate surface appear as isolated, subresolution, bright spots (Fig. 2 *A*). These accumulate uniformly on the surface (Fig. 2 *B*). Then, dark patches appear, even as the intensity in surrounding regions continues to increase (Fig. 2 *C*). The dark patches are not simply dark compared to their surroundings; their absolute intensity is lower than before. That is, they are regions from which lipid has been lost. Dark patches nucleate, spread, and coalesce (Fig. 2, *D–G*) until they fill the entire field of view (Fig. 2 *H*). Fluorescence recovery after photobleaching (see below) indicated that dark patches were SLB.

Fluorescence intensity provides a quantitative and spatially resolvable measure of adsorbed lipid that clearly distinguishes phases in the SLB formation process above (Fig. 3). After a transient ($\leq$10 min) increase in intensity, when pure buffer was replaced with buffer containing labeled vesicles, the fluorescence intensity continued to increase. This is the phase dominated by vesicle adsorption. The rate of increase was constant at first, and then accelerated. In this second (accelerating) phase, SLB patches appeared. A peak in the intensity defines the beginning of a third phase, dominated by SLB patch spreading, during which the intensity rapidly decayed to a final value that was spatially uniform (standard deviation $<$7% of the mean).

To reliably interpret fluorescence intensity as a measure of lipid on the surface, it was necessary to subtract the contribution from lipid in the bulk. This was done based on rinsing with vesicle-free buffer after SLB formation was complete (Fig. 3, ~45 min after peak intensity). Averaged over a large area (50 μm diameter), intensity during the rinse decayed exponentially. The inverse of this decay profile, along with the camera dark level, was subtracted from the average intensity at all prerinse time points to yield a correct measure of the surface fluorescence (see the Supporting Material).

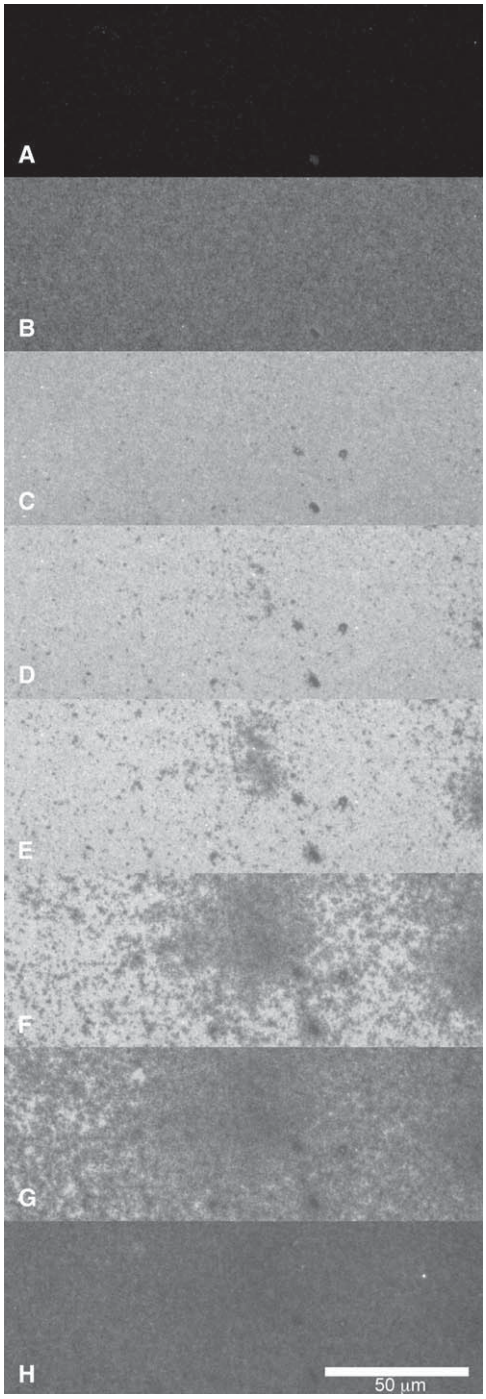

FIGURE 2 Fluorescence video microscopy of vesicles adsorbing and rupturing to form a supported lipid bilayer (see Movie S1). (*A–H*) Sample frames taken at successive time points marked by corresponding letters in Fig. 3. The field of view brightens as vesicles adsorb to the glass surface (*A* and *B*). Dark patches appear where vesicles rupture to form SLB whereas, elsewhere, vesicles continue to adsorb (*C*). SLB patches continue to nucleate and spread (*D–G*) until the entire surface is covered in SLB (*H*).

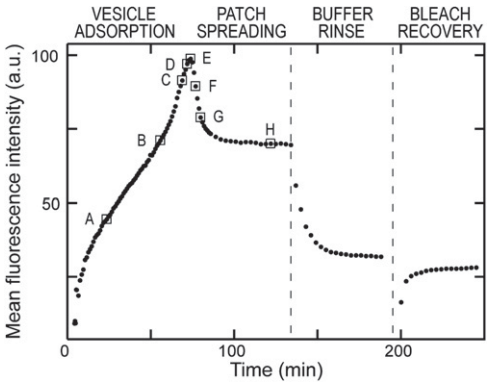

FIGURE 3 Mean intensity versus time for a representative sample. Lettered points correspond to images in Fig. 2. Mean intensity increases quickly at first, as buffer is replaced by fluorescent vesicle suspension, then more slowly, as vesicles adsorb on the substrate, then quickly again. It is in this late phase of accelerating adsorption that resolvable patches of SLB first appear (see Fig. 2, *C* and *D*). As patches spread, the mean intensity reaches a maximum and drops rapidly to a stable value. The fluorescent vesicle suspension is then replaced by buffer and the associated decrease in intensity provides an in situ measure of the bulk fluorescence. Finally, the sample is photobleached to test the mobility and continuity of lipid on the surface.

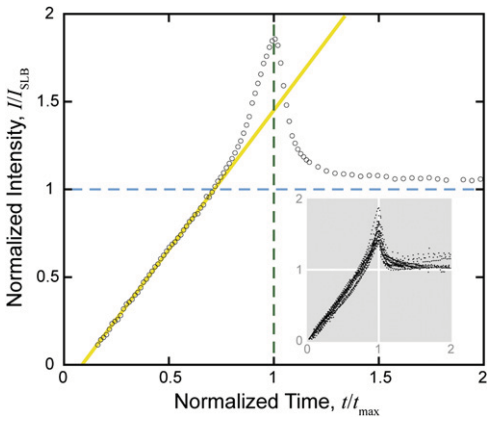

FIGURE 4 Mean intensity (corrected for background and normalized to I_{SLB}; see the Supporting Material) versus time (normalized to t_{max}) for all 16 concentrations (*inset*) and for one, representative sample (same as in Fig. 3). All samples exhibit a linear increase in intensity at early times (the least-squares linear fit for $I/I_{SLB} < 0.8$ is highlighted and extended in *yellow*). This is followed by a period of accelerating adsorption that ends abruptly. From its maximum, intensity decreases rapidly as the SLB becomes continuous and vesicles desorb. At the highest concentrations, some vesicles remain adsorbed to the bilayer (until rinsed away with lipid free buffer) causing intensity levels to hover above I_{SLB} toward the end of the time range depicted.

After the buffer rinse, the surface fluorescence was constant for at least 1 h and its magnitude was consistent from sample to sample, independent of the vesicle concentration during adsorption. Furthermore, in every sample tested, a bleached spot recovered >90% of its original fluorescence (Fig. 3), indicating the presence of a continuous, fluid SLB on the surface, from which the lipid does not get rinsed away. The <10% immobile fraction is likely due to the presence of vesicles trapped in the bilayer.

The average, corrected fluorescence intensity data, $I(t)$, from 16 independent experiments at different lipid concentrations (1.5–20 μg/mL) collapse onto a single curve on rescaling time and intensity (Fig. 4, *inset*). Its characteristic time course has three outstanding features, corresponding to the three phases described above: i), it begins with a linear rise up to an intensity $I \sim 0.8\, I_{SLB}$; ii), it accelerates; and then iii), it drops, rapidly at first, to a final, constant level (Fig. 4).

Quantitative aspects and their concentration dependence are summarized in Fig. 5. The initial linear rise is faster at higher concentrations (Fig. 5 *A*) and the combined duration of the linear and accelerating adsorption phases (i.e., the time, t_{max}, required to reach the maximum average intensity, I_{max}) is inversely related to concentration (Fig. 5 *B*), suggesting that in both phases, adsorption is a first-order reaction. The abrupt decrease in intensity after t_{max} has a characteristic (1/e) time, 3 min $> \tau >$ 9 min, which also depends on concentration (Fig. 5 *C*), suggesting that the mechanism of lipid loss is sensitive to details of how it adsorbed. The maximum average intensity, I_{max}, varies from 30% to 70% above the final intensity, I_{SLB}, but is not correlated with concentration (Fig. 5 *D*). This variability across samples is significantly greater than the variability in I_{max} from region to region within a sample (see the Supporting Material), suggesting that the amount of excess lipid adsorbed is controlled by fluctuations in the adsorption process.

A steady and then accelerating increase in intensity that switches abruptly to a rapid decrease is also seen at higher spatial resolution, albeit with varying values of t_{max} and I_{max} (Fig. 6). In Fig. 6 *A*, each horizontal line is the intensity profile of the same linear region on the surface (1 pixel $\times$ 167 μm) at 1-min intervals. The prominent triangular dark regions decorating the light-dark boundary mark intensity drops, which originate at a point and extend laterally, indicating that SLB patches can grow by spreading. Roughness of the light-dark boundary indicates that new SLB patches nucleate, at the same time as existing SLB patches spread and coalesce. Some regions lose intensity while adjacent regions continue to brighten, suggesting that the transformation from vesicle to SLB is not tightly coupled to the density of lipid on the surface.

DISCUSSION

We have used fluorescence microscopy to observe in detail how DMPC vesicles accumulate on a glass surface and transform into a uniform, continuous, fluid SLB. Earlier work has shown that the SLB formed on silica has the mass (10–12) and thickness (12,13) of a single bilayer. In our experiments, we used borosilicate glass, since it is the standard for microscopy and easier to handle than silica. The conditions for SLB formation on silica and borosilicate are similar (34) and result in the same amount of adsorbed lipid (K. Weirich,

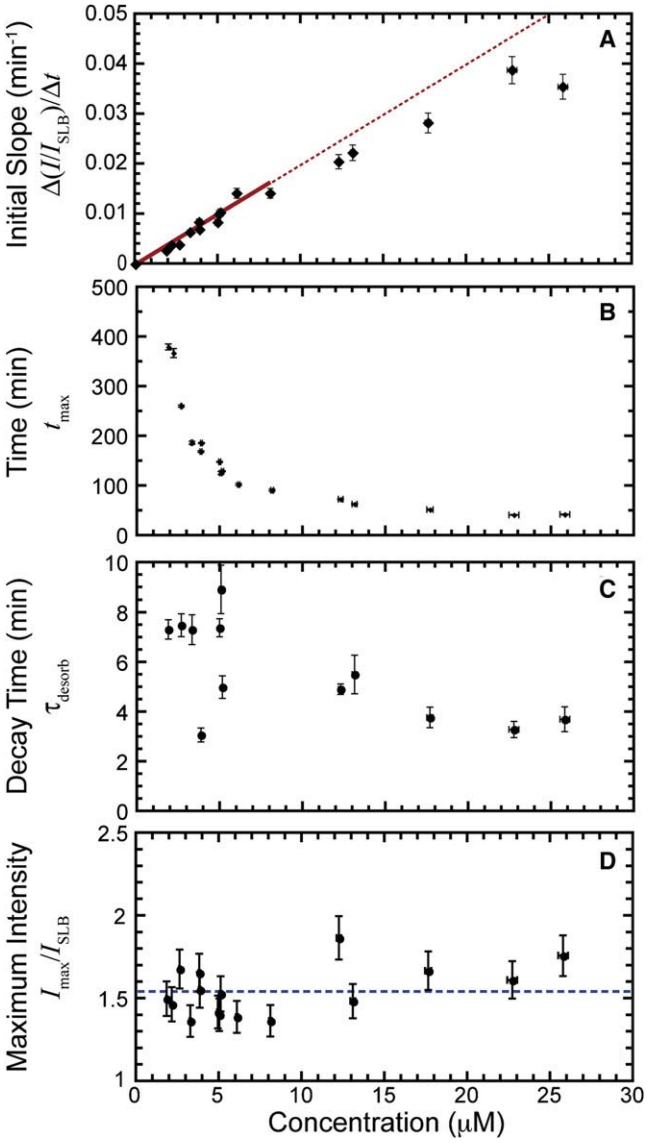

FIGURE 5 Quantitative characteristics of the time course of mean intensity, $I(t)$, as a function of bulk lipid concentration. (*A*) The initial rate of adsorption (slope of the linear fit for $I/I_{SLB} < 0.8$) is directly proportional to concentration at all but the highest concentrations. (*B*) The time to maximum mean intensity is inversely dependent on concentration. (*C*) The characteristic time of an exponential fit to the rapid decrease after maximum intensity is weakly dependent on concentration. (*D*) The maximum intensity varies, but is not sensitive to concentration. (See the Supporting Material for a comparison of the variability of I_{max} within a sample and across samples at different concentrations.) Horizontal error bars are based on reproducibility of bulk fluorimetry measurements (M.S.E. for $n = 9$). Vertical error bars are based on the video sampling rate for time measurements and the uncertainty in the measured background for intensity measurements.

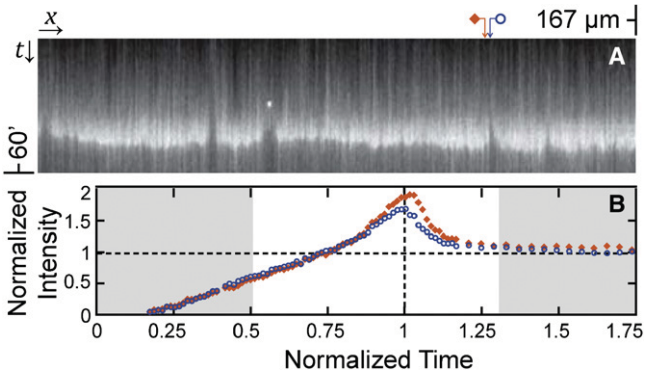

FIGURE 6 Spatial variation in the time evolution of surface fluorescence. (*A*) Successive intensity traces along a horizontal line (taken at 1-min intervals) are arrayed vertically, revealing triangular dark (bilayer-covered) regions along the bright-dark interface, which attest to the tendency for SLB patches to spread via edge-induced rupture. (*B*) Despite similar initial adsorption rates, neighboring regions (1 μm diameter, centers indicated by symbols in *A*) reach different maximum intensities before forming SLB.

unpublished data) indicating that the SLB on borosilicate is also a single bilayer.

Our results reveal six important features of the SLB formation process: i), vesicles rearrange on the substrate before rupture; ii), vesicles have greater affinity for SLB edges than for glass; iii), vesicles have a lower affinity for the SLB surface than for glass; iv), SLB formation culminates in the rapid and widespread desorption of vesicles; v), isolated vesicle rupture is rare; and vi), SLB edges catalyze vesicle rupture. Here, we elaborate on the reasoning that supports these conclusions, discuss correspondence with earlier studies, and comment on implications for future experiments and modeling.

Vesicles rearrange on the substrate before rupture

Throughout the range of lipid concentrations tested, adsorption proceeds at a constant rate up to a relatively large lipid surface density of ~0.8 I_{SLB} (Fig. 4). This is remarkable because a finite substrate might be expected to impose saturation kinetics, resulting in a strictly declining adsorption rate (35,36). Even if no vesicles ruptured during adsorption, and adsorbed vesicles remained perfectly spherical (thereby presenting four times more lipid per unit area than SLB), saturation kinetics would have imposed a 20% reduction in the rate of adsorption at a lipid surface density of ~0.8 I_{SLB}, which would have been easily detectable.

The sustained period of constant adsorption indicates that either adsorbed lipid is rearranging on the surface (35,36), or lipid on the surface enhances vesicle adsorption in a manner that precisely compensates for saturation. In the first case, a vesicle approaching an occupied site is not prevented from adsorbing because thermal motion (vesicles rolling or SLB patches crawling) on the surface liberates the site before the incident vesicle has diffused back into the bulk. AFM studies have explicitly noted the absence of such thermal motion (12,15), but this may have been a consequence of Ca^{2+} ions mediating binding between lipid and substrate. In a recent study, Klacar et al. (37) argued on theoretical grounds that diffusive motion of adsorbed lipid is to be

expected in the absence of Ca^{2+} ions, although a moderate density of pinning sites could suppress it. Neither Ca^{2+} nor any other divalent cation was present in our experiments. In the second case, the presence of lipid on the surface increases the binding affinity for vesicles, such that the accelerated adsorption perfectly balances the effect of saturation. Although some lipid-dependent increase in binding affinity is necessary to explain the phase of accelerating adsorption, as discussed in the next section, it seems unlikely that such precise compensation would sustain over such a large proportion of the adsorption process. It further seems unlikely that this precise compensation would be unaffected by bulk lipid concentration.

Vesicles have a greater affinity for SLB edges

After a prolonged and steady rise, the amount of lipid on the glass surface accumulates even faster before rapidly decreasing to a final, constant value. This acceleration in adsorption can only be explained by the emergence of a new substrate for which vesicles have a greater affinity than bare glass. We posit the new substrate to be SLB edges, essential and transient byproducts of vesicle rupture. Image data correlates with spatially averaged intensity data in a manner consistent with this idea. First, relatively small SLB patches are clearly present in images taken during the phase of accelerating adsorption, but rarely before (Figs. 2 and 3). Second, during the phase of rapidly declining surface intensity, large SLB patches spread and coalesce. The associated loss of SLB edges, a substrate with high affinity for vesicle binding, and resulting dominance of SLB, a substrate with even lower affinity for vesicles than glass (see below), readily explains the decrease in intensity as the result of vesicles desorbing back into solution. The abruptness of this transition then corresponds to the sudden decline in SLB edges as SLB patches spread to the point of contact and coalesce (Fig. 7) and the slower desorption that follows results from vesicles being ejected from the edges of holes in the SLB as it reaches completion.

Vesicles have a lower affinity for the SLB surface than for glass

After the rapid decline in intensity during the final stage of SLB formation, the magnitude of dI/dt, if not zero, is a factor of ≥ 10 lower than it is during the period of constant adsorption. The sign of this residual change in fluorescence intensity depends on the bulk concentration of vesicles; it can be negative, as vesicles desorb from the SLB surface at the lower bulk concentrations, or positive, as vesicles adsorb at the higher bulk concentrations. The affinity of vesicles for SLB surface is therefore significantly less than for glass. Based on our experimental conditions (vesicle diameter, ~50 nm; lipid mass, ~677 g/mol; and lipid concentration range, (1.5–20 μg/mL)), $K_D \sim 1$ nM for vesicles on an SLB surface.

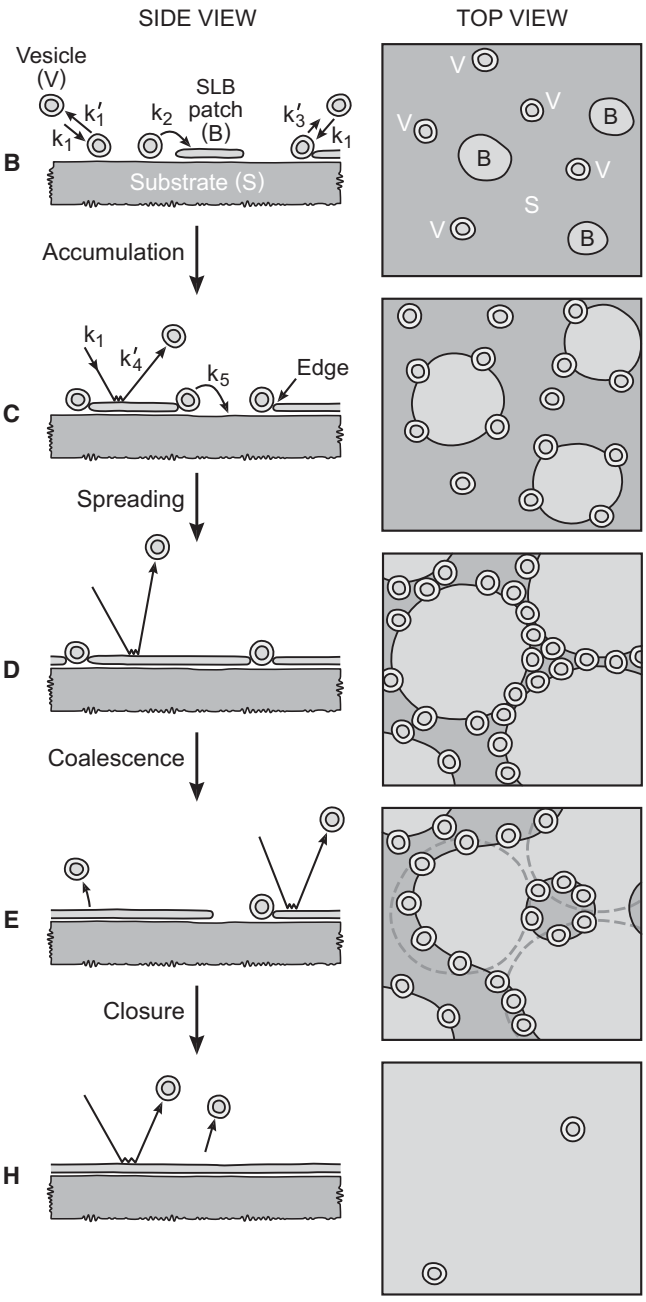

FIGURE 7 Proposed stages of SLB formation from vesicles (labeled in correspondence with Figs. 2 and 3). (*B*) Vesicles accumulate on the substrate and, in isolation, rupture slowly into patches of SLB. (*C*) Vesicles accumulate preferentially along edges of SLB patches, where they rupture more quickly and fuse with the adjacent SLB patch. (*D* and *E*) SLB coverage reaches a critical point, or percolation limit, where liquid-like coalescence of patches occurs rapidly (at constant bilayer area), abruptly decreasing the total edge length and releasing vesicles into solution. Modeling the associated kinetics requires six rate constants: three reflecting vesicles' higher affinity for bilayer edge than for glass than for bilayer surface ($k_3' < k_1' < k_4'$), and three more for adsorption (k_1), isolated rupture (k_2), and edge-bound rupture ($k_5 > k_2$) of vesicles.

SLB formation culminates in rapid and widespread vesicle desorption

At all vesicle concentrations tested, lipid accumulated on the surface in excess of that needed for the final SLB and then rapidly left the surface in the final phase of the SLB formation process. The simplest explanation is that excess lipid adsorbed and later desorbed in the form of unruptured vesicles (Fig. 7). This explanation is consistent with the results of earlier studies using complementary techniques.

QCM-D studies of SLB formation detect both the mass and structure of adsorbed material through changes in resonant frequency and dissipation, respectively (12,15,19,21–24). A rapid increase and subsequent decrease in dissipation is characteristic of SLB formation and a similar surge and loss of adsorbed mass is seen under most conditions. These transients have been interpreted as indicating cooperative rupture of adsorbed vesicles at a critical surface density, the decrease in mass being attributed to the release of water from the interior of rupturing vesicles. However, such transients are also consistent with mass being lost in the form of whole (unruptured) vesicles because QCM-D alone cannot distinguish between lipid mass and water mass. The simultaneous QCM-D and surface plasmon resonance measurements of Reimhult et al. (22,23) have shown that desorption of lipid does contribute to the mass loss detected by QCM-D. Studies of SLB formation using ellipsometry also detect lipid desorption (13).

A quantitative assessment of the relative amount of lipid and water mass loss contributing to the QCM-D signal is complicated because accounting for viscous/hydrodynamic effects (e.g., rolling vesicles) requires knowing just how the vesicle mass is coupled to the surface. Nevertheless, a rough calculation based on our observations indicates that desorption of intact vesicles can account for the decrease in frequency and dissipation reported by QCM-D. Specifically, given that DMPC (~677 g/mol) has an area per headgroup of 0.59 nm^2 (38) and a bilayer thickness of 5 nm (20), the lipid/water mass ratio in our vesicles ($d = 50$ nm) is ~1:3. If the decrease in average surface fluorescence intensity I_{max} to I_{SLB} is entirely due to desorption of such vesicles, the corresponding expected total mass loss ranges from 460–1200 ng/cm^2 (cf. the value of 380 ng/cm^2 for SLB). QCM-D under comparable conditions reports a total mass loss of ~600 ng/cm^2 (22,23).

Isolated vesicle rupture is rare

The lack of a concentration dependence in the amount of excess lipid adsorbed suggests that individual vesicle rupture is a rare event. As the time for SLB formation becomes long compared to the time for vesicles to rupture in isolation, the proportion of vesicles undergoing isolated rupture should increase and I_{max} should approach I_{SLB}. We expected to access this regime at our lowest concentrations, but saw no such trend (Fig. 5 *D*). Our longest t_{max} suggests that isolated rupture is slow compared to nearly 7 h and, thus, the fraction of vesicles undergoing isolated rupture is small. The relative dominance of edge-induced rupture is supported by the absence of fluorescence recovery after photobleaching in the uniformly bright phase immediately before dark patches appear (data not shown). In that phase, SLB patches, if present, are not continuous on resolvable length scales (~500 nm). The relative dominance of edge-induced rupture is consistent with AFM observations that PC-vesicles adsorbed to silica can remain stable for days (12,19). Contrasting reports of nearly 50% isolated rupture (17) may reflect the large proportion of fluorescent lipid molecules in that otherwise similar system.

Bilayer edges catalyze vesicle rupture

The rapid (Figs. 2 and 3) and spatially resolved (Fig. 6) spreading of bilayer patches suggests that bilayer edges catalyze vesicle rupture. Earlier studies have also implicated edge-induced rupture as a mechanism of SLB formation. Johnson et al. (17) showed that vesicles fuse more quickly with surrounding lipid when adsorbed in the presence of osmotically preruptured vesicles. Hamai et al. (18) observed that giant vesicles adsorbed to glass rupture more quickly at an SLB edge (msec) than in isolation (tens of min). Richter et al. (19) proposed edge-induced rupture as an alternative to the critical vesicle density hypothesis based on AFM data.

CONCLUSIONS

Fluorescence microscopy of dilute DMPC vesicle suspensions in contact with borosilicate substrates has revealed new aspects of supported lipid bilayer formation. In particular, vesicle adsorption accelerates (rather than saturates) as SLB patches appear and spread. The acceleration is followed by an abrupt decrease when excess lipid is ejected from the surface as SLB patches spread and coalesce. These features suggest that vesicles have high affinity for an increasing and subsequently decreasing amount of SLB edge. The tendency of SLB patches to spread and the variability in the maximum amount of lipid on the surface immediately before SLB formation both argue against a critical vesicle density required for rupture. The desorption of vesicles upon SLB patch coalescence provides an alternative explanation for QCM-D data.

The long-range goal to which this research contributes is a detailed understanding of vesicle adsorption and SLB formation on glass. Ideally, this understanding would be represented in a mathematical model whose analytical solution would predict measurable features of the formation process and enable its engineering. Our data suggests a simple model with three types of vesicle binding sites (Fig. 7): i), bare glass, a site of standard affinity; ii), SLB edge, a site of high affinity whose appearance correlates with the acceleration of vesicle adsorption to the surface and whose disappearance correlates with the rapid desorption of vesicles in the final stages of SLB formation (Fig. 4); and iii), SLB itself, a low affinity site to which vesicles only adsorb at the highest concentrations in this study. The data further suggest the presence of two different rates for vesicle rupture, one for vesicles on glass (Fig. 7, k_2) and

a different, faster, one for vesicles bound to SLB edge (Fig. 7, k_5), to explain the tendency of SLB patches to spread (Fig. 6). The resulting set of coupled differential equations does not appear to be solvable by analytical methods (M. Dougherty, University of California, Santa Barbara, personal communication, 2009), but numerical methods that attempt to fit $I(t)$ should yield estimates of rate constants (in progress). If models can yield useful estimates of the rate constants for vesicle adhesion and rupture, future experiments might compare the effect of surface charge or counterions on these processes to gain greater control over the SLB formation process.

SUPPORTING MATERIAL

Methods and results, five figures, and a movie are available at http://www.biophysj.org/biophysj/supplemental/S0006-3495(09)01564-1.

This work was supported in part by Corning.

REFERENCES

1. Schmitz, J., and K. E. Gottschalk. 2008. Mechanical regulation of cell adhesion. *Soft Matter*. 4:1373–1387.
2. Mukhopadhyay, R., H. W. G. Lim, and M. Wortis. 2002. Echinocyte shapes: bending, stretching, and shear determine spicule shape and spacing. *Biophys. J*. 82:1756–1772.
3. Hamill, O. P., and B. Martinac. 2001. Molecular basis of mechanotransduction in living cells. *Physiol. Rev*. 81:685–740.
4. Suzuki, H., and S. Takeuchi. 2008. Microtechnologies for membrane protein studies. *Anal. Bioanal. Chem*. 391:2695–2702.
5. Brian, A. A., and H. M. McConnell. 1984. Allogenic stimulation of cyto-toxic T-cells by supported planar membranes. *Proc. Natl. Acad. Sci. USA*. 81:6159–6163.
6. Tamm, L. K., and H. M. McConnell. 1985. Supported phospholipid bilayers. *Biophys. J*. 47:105–113.
7. Yang, T. L., S. Y. Jung, …, P. S. Cremer. 2001. Fabrication of phospholipid bilayer-coated microchannels for on-chip immunoassays. *Anal. Chem*. 73:165–169.
8. Gong, M., S. Yang, …, Y. K. Gong. 2008. Surface modification of biomedical materials with cell membrane mimetic structures. *Prog. Chem*. 20:1628–1634.
9. Kalb, E., S. Frey, and L. K. Tamm. 1992. Formation of supported planar bilayers by fusion of vesicles to supported phospholipid monolayers. *Biochim. Biophys. Acta*. 1103:307–316.
10. Keller, C. A., and B. Kasemo. 1998. Surface specific kinetics of lipid vesicle adsorption measured with a quartz crystal microbalance. *Biophys. J*. 75:1397–1402.
11. Nollert, P., H. Kiefer, and F. Jähnig. 1995. Lipid vesicle adsorption versus formation of planar bilayers on solid surfaces. *Biophys. J*. 69:1447–1455.
12. Richter, R., A. Mukhopadhyay, and A. Brisson. 2003. Pathways of lipid vesicle deposition on solid surfaces: a combined QCM-D and AFM study. *Biophys. J*. 85:3035–3047.
13. Stroumpoulis, D., A. Parra, and M. Tirrell. 2006. A kinetic study of vesicle fusion on silicon dioxide surfaces by ellipsometry. *AIChE J*. 52:2931–2937.
14. Horn, R. G. 1984. Direct measurement of the force between 2 lipid bilayers and observation of their fusion. *Biochim. Biophys. Acta*. 778:224–228.
15. Richter, R. P., and A. R. Brisson. 2005. Following the formation of supported lipid bilayers on mica: a study combining AFM, QCM-D, and ellipsometry. *Biophys. J*. 88:3422–3433.
16. Reviakine, I., and A. Brisson. 2000. Formation of supported phospholipid bilayers from unilamellar vesicles investigated by atomic force microscopy. *Langmuir*. 16:1806–1815.
17. Johnson, J. M., T. Ha, …, S. G. Boxer. 2002. Early steps of supported bilayer formation probed by single vesicle fluorescence assays. *Biophys. J*. 83:3371–3379.
18. Hamai, C., P. S. Cremer, and S. M. Musser. 2007. Single giant vesicle rupture events reveal multiple mechanisms of glass-supported bilayer formation. *Biophys. J*. 92:1988–1999.
19. Richter, R. P., R. Bérat, and A. R. Brisson. 2006. Formation of solid-supported lipid bilayers: an integrated view. *Langmuir*. 22:3497–3505.
20. Schönherr, H., J. M. Johnson, …, S. G. Boxer. 2004. Vesicle adsorption and lipid bilayer formation on glass studied by atomic force microscopy. *Langmuir*. 20:11600–11606.
21. Reimhult, E., F. Hook, and B. Kasemo. 2003. Intact vesicle adsorption and supported biomembrane formation from vesicles in solution: influence of surface chemistry, vesicle size, temperature, and osmotic pressure. *Langmuir*. 19:1681–1691.
22. Reimhult, E., C. Larsson, …, F. Höök. 2004. Simultaneous surface plasmon resonance and quartz crystal microbalance with dissipation monitoring measurements of biomolecular adsorption events involving structural transformations and variations in coupled water. *Anal. Chem*. 76:7211–7220.
23. Reimhult, E., M. Zäch, …, B. Kasemo. 2006. A multitechnique study of liposome adsorption on Au and lipid bilayer formation on SiO2. *Langmuir*. 22:3313–3319.
24. Seantier, B., C. Breffa, …, G. Decher. 2005. Dissipation-enhanced quartz crystal microbalance studies on the experimental parameters controlling the formation of supported lipid bilayers. *J. Phys. Chem. B*. 109:21755–21765.
25. Benes, M., D. Billy, …, W. T. Hermens. 2004. Surface-dependent transitions during self-assembly of phospholipid membranes on mica, silica, and glass. *Langmuir*. 20:10129–10137.
26. Wang, S. T., M. Fukuto, and L. Yang. 2008. In situ x-ray reflectivity studies on the formation of substrate-supported phospholipid bilayers and monolayers. *Phys. Rev. E*. 77:031909-1–031909-8.
27. Gutberlet, T., B. Klosgen, …, R. Steitz. 2004. Neutron reflectivity as method to study in-situ adsorption of phospholipid layers to solid-liquid interfaces. *Adv. Eng. Mater*. 6:832–836.
28. Hope, M. J., M. B. Bally, …, P. R. Cullis. 1985. Production of large unilamellar vesicles by a rapid extrusion procedure - characterization of size distribution, trapped volume and ability to maintain a membrane-potential. *Biochim. Biophys. Acta*. 812:55–65.
29. Stewart, J. C. M. 1980. Colorimetric determination of phospholipids with ammonium ferrothiocyanate. *Anal. Biochem*. 104:10–14.
30. Yoshida, Y., E. Furuya, and K. Tagawa. 1980. A direct colorimetric method for the determination of phospholipids with dithiocyanatoiron reagent. *J Biochem*. 88:463–468.
31. Albrink, M. J. 1959. The microtitration of total fatty acids of serum, with notes on the estimation of triglycerides. *J. Lipid Res*. 1:53–59.
32. Bligh, E. G., and W. J. Dyer. 1959. A rapid method of total lipid extraction and purification. *Can. J. Biochem. Physiol*. 37:911–917.
33. Reference deleted in proof.
34. Anderson, T. H., Y. J. Min, …, J. N. Israelachvili. 2009. Formation of supported bilayers on silica substrates. *Langmuir*. 25:6997–7005.
35. Taylor, J. B., and I. Langmuir. 1933. The evaporation of atoms, ions, and electrons from caesium films on tungsten. *Phys. Rev*. 44:423–458.
36. Masel, R. I. 1996. Principles of Adsorption and Reaction on Solid Surfaces. John Wiley & Sons, New York. 377–383.
37. Klacar, S., K. Dimitrievski, and B. Kasemo. 2009. Influence of surface pinning points on diffusion of adsorbed lipid vesicles. *J. Phys. Chem. B*. 113:5681–5685.
38. Koenig, B. W., H. H. Strey, and K. Gawrisch. 1997. Membrane lateral compressibility determined by NMR and x-ray diffraction: effect of acyl chain polyunsaturation. *Biophys. J*. 73:1954–1966.